Crystals 2022

MDPI

*Proceedings*

# Photovoltaic properties and microstructures of polysilane-added perovskite solar cells

**Shinichiro Mizuno [1], Takeo Oku [1]*, Atsushi Suzuki [1], Masanobu Okita [2], Sakiko Fukunishi [2], Tomoharu Tachikawa [2], and Tomoya Hasegawa [2]**

[1] Department of Materials Science, The University of Shiga Prefecture, 2500 Hassaka, Hikone, Shiga 522-8533, Japan; oe21smizuno@ec.usp.ac.jp (S.M.); suzuki@mat.usp.ac.jp (A.S.)
[2] Osaka Gas Chemicals Co., Ltd., 5-11-61 Torishima, Konohana-ku, Osaka 554-0051, Japan; okita@ogc.co.jp (M.O.); fukunishi@ogc.co.jp (S.F.); t-tachikawa@ogc.co.jp (T.T.); hasegawa_tomoya@ogc.co.jp (T.H.)
* Correspondence: oku@mat.usp.ac.jp; Tel.: +81-749-28-8368

**Abstract:** $CH_3NH_3PbI_3$ perovskite photovolt aic devices treated with a polysilane layer were fabricated and characterized. Decaphenylcyclopentasilane (DPPS) in chlorobenzene solution was spin-coated between the perovskite layer and the hole transport layer of spiro-OMeTAD, and the resulting device was annealed at 190 °C. The DPPS-treated devices had higher conversion efficiencies than the standard one and they were stable in ambient air. Microstructural observations suggested that DPPS would work effectively a bulk-hetero structure along with perovskite layers.

**Keywords:** Perovskite; solar cell; polysilane; microstructure

## 1. Introduction

Perovskite solar cells are attracting attention as an alternative to silicon solar cells, which are currently the most widely studied [1-7]. Silicon solar cells have high conversion efficiency, but there are challenges in terms of cost and weight. Perovskite solar cells are generally characterized by high conversion efficiency, low cost, and ease of fabrication process [8-10]. However, these lead halide compounds are typically unstable in air [11-13], and the stability of the corresponding perovskite photovoltaic devices should be improved for inclusion in the actual cell module [14-17].

The instability of perovskite photovoltaic devices results from the migration of $CH_3NH_3$ (MA) and iodine (I) and reactivity with $H_2O$ [18-23]. To improve the stability of perovskite photovoltaic devices, polymeric materials and organic semiconductors have been investigated [24-26]. For instance, in polymeric materials, poly(ethylene oxide), poly(ethylene glycol) and poly(propylene carbonate) have been used to protect the perovskite layer from oxygen and moisture [27,28] and to enhance stability. Both polymeric materials formed cross-linked networks comprising perovskite grains, which suppressed defects. Methods was also developed to ensure long-term stability by passivating the grain boundaries of perovskite grains using Lewis acid bases and functional groups to increase the activation energy of decomposition [29-31].

A type that is introduced between the perovskite layer and the hole transport layer to improve long-term stability and photovoltaic properties has also been studied, and polysilane derivatives are being considered [32-35]. Polysilane derivatives exhibit two important advantages. The first relates to polysilanes being *p*-type semiconductors that facilitate hole transfer and rectification at the *pn* junction [36,37]. The second derives from polysilanes having high stabilities at elevated temperatures up to ~300 °C and are therefore expected to act as a protective layer across the perovskite surface. In addition, polysilanes have been applied to perovskite solar cells, and the photovoltaic properties were improved, especially by adding decaphenylcyclopentasilane (DPPS) [33-35]. The DPPS-

**Citation:** Lastname, F.; Lastname, F.; Lastname, F. Title. *Chem. Proc.* **2021**, *3*, x. https://doi.org/10.3390/xxxxx

Published: date

doped devices reported so far are based on spin-coating of DPPS on the perovskite layer using the anti-solvent method, and it is necessary to focus on the morphology of the interface involved in the stability and carrier transport.

The purpose of the present work is to investigate the photovoltaic properties, stabilities and microstructure of DPPS-treated $MAPbI_3$ perovskite solar cells. In this study, the perovskite layer was formed by annealing the film at 140 °C or 190 °C and DPPS was treated by an anti-solvent method. The effects of DPPS treatment on the photovoltaic properties, stability and microstructure of $MAPbI_3$ perovskite solar cells were investigated using current density voltage (*J-V*) characteristics, X-ray diffraction (XRD) and transmission electron microscopy (TEM).

## 2. Experimental Procedure

Figure 1 (a) shows a schematic diagram of the completed device. All fabrication processes were performed under atmospheric conditions in ambient air [38,39], and the temperature and humidity were ~25 °C and ~50 %, respectively. F-doped tin oxide (FTO, Nippon Sheet Glass Company, Tokyo, Japan, ~10 Ω/) substrates were cleaned with methanol and acetone in an ultrasonic bath and an ultraviolet ozone cleaner (Asumi Giken, Tokyo, Japan, ASM401N). Next, 0.15 and 0.30 M precursor solutions of $TiO_2$ compact layers were prepared from 1-butanol (Wako Pure Chemical Industries, Osaka, Japan) and titanium diisopropoxide bis(acetylacetonate) (Sigma Aldrich, Tokyo, Japan). These precursor solutions of compact $TiO_2$ were spin-coated on the FTO substrate at 3000 rpm for 30 s, and the substrates were annealed at 125 °C for 5 min. To form a uniform, compact $TiO_2$ layer, the 0.30 M precursor solution was spin-coated twice. Next, the FTO substrate was annealed at 550 °C for 30 min to form the compact $TiO_2$ layer. After that, a $TiO_2$ paste (precursor solution for mesoporous $TiO_2$) was spin-coated on the compact $TiO_2$ layer at 5000 rpm for 30 s. This $TiO_2$ paste was prepared by mixing distilled water (0.5 mL), poly (ethylene glycol) PEG-20000 (Nacalai Tesque, Kyoto, Japan, PEG #20000, 20 mg), and $TiO_2$ powder (Aerosil, Tokyo, Japan, P-25, 200 mg). This solution was further mixed with the surfactant Triton X-100 (Sigma Aldrich, 10 μL) and acetylacetone (Wako Pure Chemical Industries, 20 μL) for 30 min, and it was left untouched for 24 h to remove bubbles in the solution. To form the mesoporous $TiO_2$ layer, the $TiO_2$-coated substrates were annealed at 550 °C for 30 min.

To prepare the perovskite compounds, solutions of $PbCl_2$ (Sigma Aldrich, Tokyo, Japan, 111.2 mg) and $CH_3NH_3I$ (Tokyo Chemical Industry, 190.8 mg) with the desired molar ratio were mixed in *N,N*-dimethylformamide (Sigma Aldrich, 0.5 mL) at 60 °C for 24 h [ ]. These perovskite precursor solutions were normally spin-coated during the first coating. During the second and third spin-coating steps, an air-blowing method was employed, as illustrated in Figure 1 (b). The cells were maintained at 90 °C during the air-blowing. DPPS (Osaka Gas Chemicals, OGSOL SI-30-15, Osaka, Japan, 10 mg) solutions were prepared in chlorobenzene (0.5 mL) and dropped onto the perovskite layer during the last 15 s of the third spin-coating of the perovskite precursor solutions. As shown in Figure 1 (b), This process was called ***D***. The standard device was annealed at 140 °C for 20 min. The devices with DPPS layers were annealed at 190 °C for 16 min.

Then, a spiro-OMeTAD layer was formed as an HTL by spin-coating, and the spiro-OMeTAD layer was formed below the gold electrodes for all the fabricated devices in the present work. Finally, gold (Au) electrodes were formed by evaporation. All the fabricated cells in the present work were put into dark storage at a temperature of 22 °C and ~30% humidity in ambient air.

Microstructural analysis was conducted by an X-ray diffractometer (Bruker, Billerica, MA, USA, D2 PHASER) and a transmission electron microscope (FEI, Oregon, USA, Talos F200X). The surface morphologies of the perovskite layers were examined using an optical microscope (Nikon, Tokyo, Japan, Eclipse E600). The current density voltage characteristics of the fabricated devices were measured (Keysight, Santa Rosa, CA, USA, B2901A)

under a solar simulator (San-ei Electric, Osaka, Japan, XES-301S) with irradiation at 100 mW $cm^{-2}$.

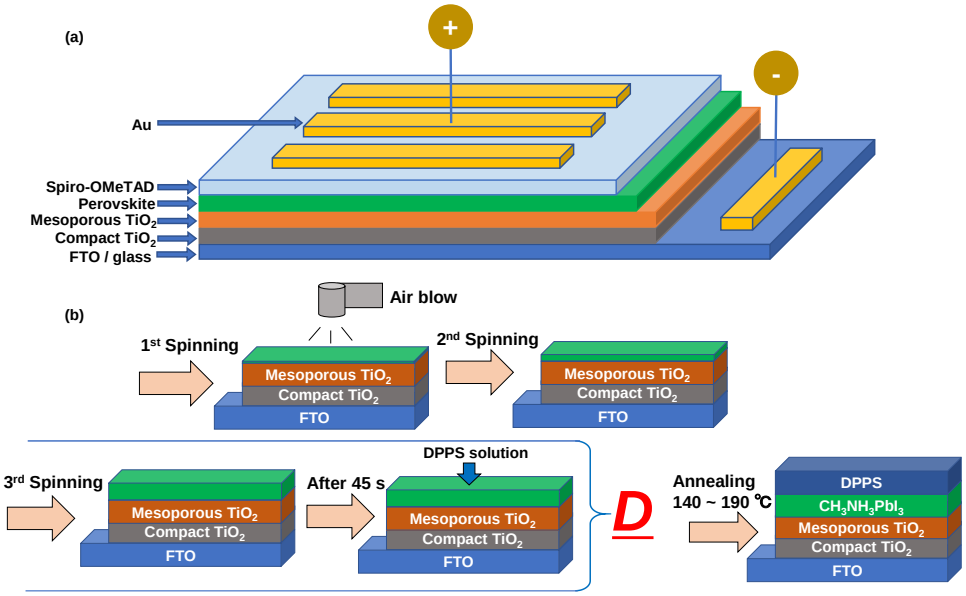


**Figure 1.** (a) Layered structure of the present solar cells (FTO / $TiO_2$ / perovskite / spiro-OMeTAD). (b) Schematic illustration detailing the processes adopted to fabricate the perovskite and DPPS layer.

## 3. Results and Discussion

Table 1 shows the photovoltaic parameters of the $TiO_2$ / perovskite / spiro-OMeTAD solar cells under illumination, which indicates the effects of the DPPS. The device without DPPS provided a short-circuit current density ($J_{SC}$) of 18.9 mA $cm^{-2}$, and a conversion efficiency (η) of 6.55 %. The $J_{SC}$ was increased from 18.9 to 23.2 mA $cm^{-2}$ by the performing the operation ***D*** 3 times, and the η increased to 11.09 %. The surface morphology of the perovskite film was improved by the operation of ***D***, indicating that DPPS blocked electrons and suppressed the recombination between a hole and an electron. XRD patterns of the perovskite solar cells showed highly (100)-oriented crystals of the perovskite compounds, which were formed by the hot air-blowing method. All devices presented few peaks corresponding to $PbI_2$, which indicated the effectiveness of the DPPS layer against high-temperature annealing at 190 °C. Among them, the smallest $PbI_2$ peak was observed for the ***D***×3 device, which indicates that DPPS suppressed the decomposition of perovskite crystals most effectively in this study. All the devices with DPPS showed a significant increase in conversion efficiency after one week, indicating that DPPS contributes to the orientation and suppression of decomposition of perovskite grains at room temperature.

**Table 1.** Measured photovoltaic parameters of solar cells.

| Devices | $J_{SC}$ (mA $cm^{-2}$) | $V_{OC}$ (V) | FF | $R_S$ (Ω $cm^{-2}$) | $R_{Sh}$ (Ω $cm^{-2}$) | $\eta$ (%) | $\eta_{ave}$ (%) |
|---|---|---|---|---|---|---|---|
| Standard | 18.9 | 0.844 | 0.410 | 5.90 | 85.3 | 6.55 | 5.19 |
| ***D***×1 | 17.0 | 0.846 | 0.443 | 5.07 | 110 | 6.38 | 5.65 |
| ***D***×2 | 21.3 | 0.696 | 0.466 | 8.38 | 290 | 6.89 | 5.36 |
| ***D***×3 | 23.2 | 0.771 | 0.620 | 5.59 | 2100 | 11.09 | 9.19 |
| ***D***×4 | 17.3 | 0.877 | 0.493 | 7.21 | 124 | 7.50 | 5.96 |

For the device with the best characteristics ***D***×3, stability measurements of the photovoltaic parameters up to 200 days were carried out. Table 2. shows the changes of parameters for ***D***×3. The device showed an increase in $\eta$ over time, with the highest η of 13.33% recorded 191 days after fabrication. DPPS and the $PbI_2$ crystal generated by the decomposition of the perovskite crystal blocked the recombination of electrons and holes, and the blocking degree reached its peak. Basically, $PbI_2$ inhibits carrier migration and degrades the photoelectric properties of the device. However, when a small amount of $PbI_2$ is added between the perovskite layer and the hole transport layer, the photoelectric properties are improved.

**Table 2.** Changes of parameters for ***D***×3.

| Time (Day) | $J_{SC}$ (mA cm$^{-2}$) | $V_{OC}$ (V) | FF | $R_S$ (Ω cm$^{-2}$) | $R_{Sh}$ (Ω cm$^{-2}$) | $\eta$ (%) | $\eta_{ave}$ (%) |
|---|---|---|---|---|---|---|---|
| As-prepared | 23.2 | 0.771 | 0.620 | 5.59 | 2100 | 11.09 | 9.19 |
| 149 days | 18.6 | 0.862 | 0.707 | 4.54 | 842 | 11.38 | 9.46 |
| 191 days | 21.4 | 0.887 | 0.701 | 5.17 | 1840 | 13.33 | 11.22 |
| 226 days | 19.3 | 0.893 | 0.701 | 5.99 | 1410 | 12.10 | 10.40 |

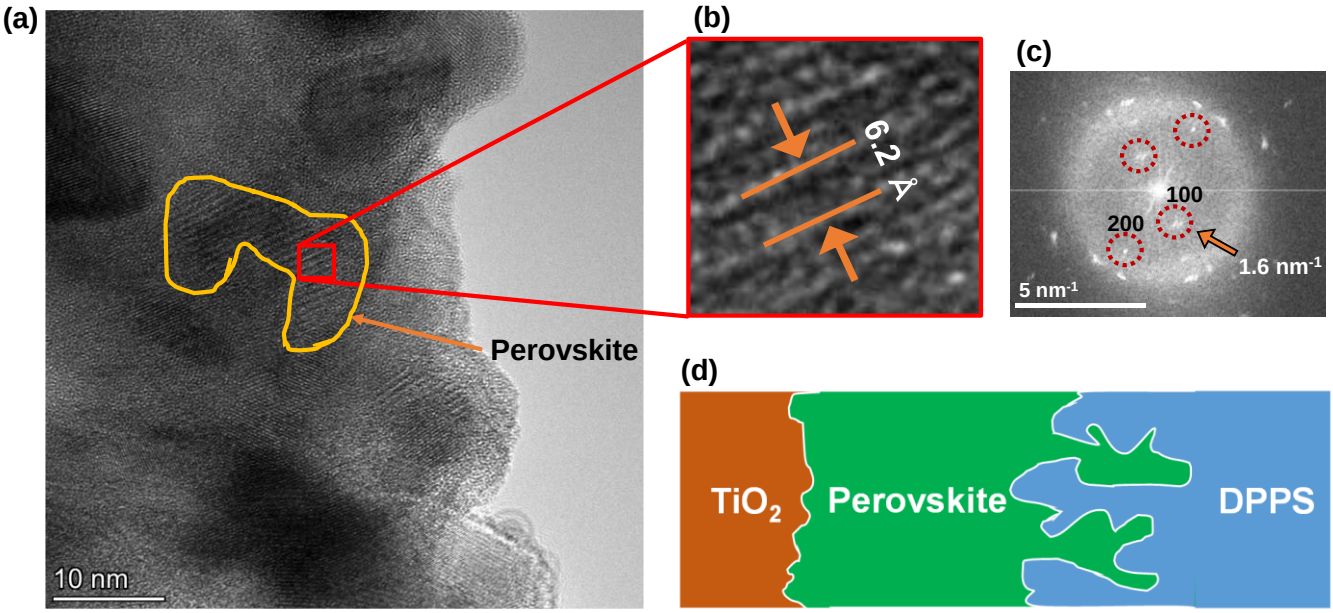


**Figure 2.** TEM observation of ***D***×3. (a) Microstructure of the perovskite-DPPS layer. (b) Enlarged image of (a). (c) FFT pattern. (d) Diagram of bulk-hetero structure.

The microstructure of the ***D***×3 device with the best characteristics was observed by transmission electron microscopy(TEM), and the results are shown in Figure 2. TEM observation revealed several types of lattice fringes. The one with a lattice distance of 6.2 Å is a perovskite crystal, and its existence can be seen from the FFT pattern. In addition, amorphous phase in the form of benzene compounds was observed around perovskite layers [30]. DPPS has an amorphous phase, so DPPS may form a bulk-hetero structure with perovskite layers.

## 4. Conclusions

In summary, $CH_3NH_3PbI_3$ perovskite photovoltaic devices treated with a polysilane layer were fabricated and characterized. It was confirmed that the insertion of the DPPS layer between the perovskite layer and the HTL improved the photovoltaic properties compared with the standard one. In particular, the device in which the operation ***D*** was performed 3 times showed the highest $J_{SC}$ and conversion efficiency immediately after the fabrication, and higher photovoltaic properties were observed even after 191 days. The presence of DPPS have contributed to the suppression of the decomposition of perovskite crystals and the smooth transport of carriers. From TEM observations, it was confirmed that there was an amorphous phase covering the perovskite crystal. This amorphous phase is considered to be DPPS and it would work effectively a bulk-hetero structure along with perovskite layers.

**Author Contributions:** Conceptualization, S.M. and T.O.; Methodology, S.M., T.O., and A.S.; Formal Analysis, S.M., T.O., and A.S.; Investigation, S.M. and T.O.; Resources, M.O., S.F., T.T., and T.H.; Data Curation, S.M. and T.O.; Writing—Original Draft Preparation, S.M. and T.O.; Writing—Review & Editing, S.M., T.O., A.S., M.O., S.F., T.T., and T.H.; Project Administration, T.O.; Funding Acquisition, T.O.

**Funding:** This research was partly funded by a Grant-in-Aid for Scientific Research (C) 21K04809.

**Conflicts of Interest:** The authors declare no conflicts of interest.

## References

1. Jiang, Q.; Zhang, L.; Wang, H.; Yang, X.; Meng, J.; Liu, H.; Yin, Z.; Wu, J.; Zhang, X.; You, J.; Enhanced electron extraction using $SnO_2$ for high-efficiency planar-structure $HC(NH_2)_2PbI_3$-based perovskite solar cells. *Nat. Energy* **2017**, *2*, 16177, doi:10.1038/nenergy.2016.177.
2. Bi, E.; Chen, H.; Xie, F.; Wu, Y.; Chen, W.; Su, Y.; Islam, A.; Gratzel, M.; Yang, X.; Han, L.; Diffusion engineering of ions and charge carriers for stable efficient perovskite solar cells. *Nat. Commun*. **2017**, *8*, 15330, doi:10.1038/ncomms15330.
3. Han, Q.; Hsieh, Y. T.; Meng, L.; Wu, J. L.; Sun, P.; Yao, E. P.; Chang, S. Y.; Bae, S. H.; Kato, T.; Bermudez, V.; High-performance perovskite/ $Cu(In,Ga)Se_2$monolithic tandem solar cells. *Science* **2018**, *361*, 904-908, doi:10.1126/science.aat5055.
4. Mei, A.; Li, X.; Liu, L.; Ku, Z.; Liu, T.; Rong, Y.; Xu, M.; Hu, M.; Chen, J.; Yang, Y.; A hole-conductor-free, fully printable mesoscopic perovskite solar cell with high stability. *Science* **2014**, *345*, 295-298, doi:10.1126/science.1254763.
5. Li, G.; Zhang, T.; Xu, F.; Zhao, Y.; A facile deposition of large grain and phase pure a-$FAPbI_3$ for perovskite solar cells via a flash crystallization. *Mater. Today Energy* **2017**, *5*, 293, doi:10.1016/j.mtener.2017.07.010.
6. Oku, T. Crystal structures of perovskite halide compounds used for solar cells. *Rev. Adv. Mater. Sci.* **2020**, *59*, 264–305, doi:10.1515/rams-2020-0015.
7. Ueoka, N.; Oku, T.; Suzuki, A. Effects of doping with Na, K, Rb, and formamidinium cations on $(CH_3NH_3)_{0.99}Rb_{0.01}Pb_{0.99}Cu_{0.01}I_{3-x}(Cl, Br)_x$ perovskite photovoltaic cells. *AIP Adv.* **2020**, *10*, 125023, doi: 10.1063/5.0029162
8. Wu, Y.; Yang, X.; Chen, W.; Yue, Y.; Cai, M.; Xie, F.; Bi, E.; Islam, A.; Han, L.; Perovskite solar cells with 18.21% efficiency and area over 1 $cm^2$ fabricated by heterojunction engineering. *Nat. Energy* **2016**, *1*, 16148, doi:10.1038/nenergy.2016.148.
9. Guerra, V. L. P.; Altamura, D.; Trifiletti, V.; Colella, S.; Listorti, A.; Giannuzzi, R.; Pellegrino, G.; Condorelli, G. G.; Giannini, C.; Gigli, G.; Implications of $TiO_2$ surface functionalization on polycrystalline mixed halide perovskite fioms and photovoltaic devices. *J. Mater. Chem*. A **2015**, *3*, 20811-20818, doi:10.1039/C5TA05220C.
10. Suzuki A.; Oe M.; Oku T., Fabrication and characterization of Ni-, Co-, and Rb-incorporated $CH_3NH_3PbI_3$ perovskite solar cells, *J. Electronic Mater.* **2021**, *50*, 1980-1995. https://doi.org/10.1007/s11664-021-08759-1.
11. Wang, R.; Mujahid, M.; Duan, Y.; Wang, Z. -K.; Xue, J.; Yang, Y.; A review of perovskites solar cell stability. *Adv. Funct. Mater.* **2019**, 1808843, doi:10.1002/adfm.201808843.
12. Hou, X.; Huang, S.; Ou-Yang, W.; Pan, L.; Sun, Z.; Chen, X.; Constructing efficient and stable perovskite solar cells via interconnecting perovskite grains. *ACS Appl. Mater. Interfaces* **2017**, *9*, 35200-35208, doi:10.1021/acsami.7b08488.
13. Ueoka, N.; Oku, T. Effects of co-addition of sodium chloride and copper (II) bromide to mixed-cation mixed-halide perovskite photovoltaic devices. *ACS Appl. Energy Mater.* **2020**, *3*, 7272–7283, doi: org/10.1021/acsaem.0c00182.
14. Lee, J. W.; Kim, S. G.; Bae, S. H.; Lee, D. K.; Lin, O.; Yang, Y.; Park, N. G.; The interplay between trap density and hysteresis in planar heterojunction perovskite solar cells. *Nano Lett*. **2017**, *17*, 4270-4276, doi:10.1021/acs.nanolett.7b01211.
15. Berhe, T. A.; Su, W. -N.; Chen, C. -H.; Pan, C. -J.; Cheng, J. -H.; Chen, H. -M.; Tsai, M. -C.; Chen, L. -Y.; Dubale, A. A.; Hwang, B. -J.; Organometal halide perovskite solar cells: degradation and stability. *Energy Environ Sci*. **2016**, *9*, 323-356, doi:10.1039/c5ee02733k.

16. Conings, B.; Drijkoningen, J.; Gauquelin, N.; Babayigit, A.; D'Haen, J.; D'Olieslaeger, L.; Ethirajan, A.; Verbeeck, J.; Manca, J.; Mosconi, E.; Intrinsic thermal instability of methylammonium lead trihalide perovskite. *Adv. Energy Mater.* **2015**, *5*, 1500477, doi:10.1002/aenm.201500477.
17. Zhang, C. C.; Li, M.; Wang, Z. K.; Jiang, Y. R.; Liu, H. R.; Yang, Y. G.; Gao, X. Y.; Ma, H.; Passivated perovskite crystallization and stability in organic-inorganic halide solar cells by doping a donor polymer. *J. Mater. Chem. A* **2017**, *5*, 2572–2579, doi:10.1039/C6TA08970D.
18. Zhao, Y.; Wei, J.; Li, H.; Yan, Y.; Zhou, W.; Yu, D.; Zhao, Q.; A polymer scaffold for self-healing perovskite solar cells. *Nat. Commun*. **2016**, *10*, 10228, doi:10.1038/ncomms10228.
19. Yang, W. S.; Park, B. W.; Jung, E. H.; Jeon, N. J.; Kim, Y. C.; Lee, D. U.; Shin, S. S.; Seo, J.; Kim, E. K.; Noh, J. H.; Iodide management in formamidinium-lead-halide-based perovskite layers for efficient solar cells. *Science* **2017**, *356*, 1376–1379, doi:10.1126/science.aan2301.
20. Lee, J. W.; Dai, Z.; Lee, C.; Lee, H. M.; Han, T. H.; De Marco, N.; Lin, O.; Choi, C. S.; Dunn, B.; Koh, J.; Tuning molecular interactions for highly reproducible and efficient formamidinium perovskite solar cells via adduct approach. *J. Am. Chem. Soc.* **2018**, *140*, 6317-6324, doi:10.1021/jacs.8b01037.
21. Jiang, J.; Wang, Q.; Jin, Z.; Polymer doping for high-efficiency perovskite solar cells with improved moisture stability. *Adv. Energy Mater.* **2018**, *8*, 1701757, doi:10.1002/aenm.201701757.
22. Seo, S.; Jeong, S.; Bae, C.; Park, N. G.; Shin, H.; Perovskite solar cells with inorganic electron- and hole-transport layers exhibiting long-term (≈500 h) stability at 85 °C under continuous 1 sun illumination in ambient air. *Adv. Mater*. **2018**, *30*, 1801010, doi: 10.1002/adma.201801010.
23. Li, M.; Wang, Z. K.; Kang, T.; Yang, Y.; Gao, X.; Hsu, C. S.; Li, Y.; Liao, L. S.; Graphdiyne-modified cross-linkable fullerene as an efficient electron-transporting layer in organometal halide perovskite solar cells. *Nano Energy* **2018**, *43*, 47–54, doi:10.1016/j.nanoen.2017.11.008.
24. Chen, Q.; De Marco, N.; Yang, Y.; Song, T. -B.; Chen, C. C.; Zhao, H.; Hong, Z.; Zhou, H.; Yang, Y.; Under the spotlight the organic-inorganic hybrid halide perovskite for optoelectronic applications. *Nano Today* **2015**, 10, 355-396, doi:10.1016/j.nantod.2015.04.009
25. Xiang, W.; Chen, Q.; Wang, Y.; Liu, M.; Huang, F.; Bu, T.; Wang, T.; Cheng, Y. B.; Gong, X.; Zhong, J.; Improved air stability of perovskite hybrid solar cells via blending poly(dimethylsiloxane)-urea copolymers. *J. Mater. Chem. A* **2017**, *5*, 5486–5494, doi:10.1039/C7TA00589J.
26. Wang , K.; Zheng, L.; Zhu, T.; Liu, L.; Becker, M. L.; Gong, X.; High performance perovskites solar cells by hybrid perovskites co-crystallized with poly(ethylene oxide). *Nano Energy* **2020**, *67*, 104229, doi:10.1016/j.nanoen.2019.104229.
27. Han, T.H.; Lee, J.W.; Choi, C.; Tan, S.; Lee, C.; Zhao, Y.; Dai, Z.; Marco, N.D.; Lee, S.J.; Bae, S.H.; Yuan, Y.; Mo Lee, H.; Yu Huang and Yang, Y.; Perovskite-polymer composite cross-linker approach for highly-stable and efficient perovskite solar cells. *Nat. Commun*. **2019**, *10*, 520, doi:10.1038/s41467-019-08455-z.
28. Wang, R.; Xue, J.; Meng, L.; Lee, J.; Zhao, Z.; Sun, P.; Cai, L.; Huang, T.; Wang, Z.; Wang, Z. K.; Duan, Y.; Yang, J. L.; Tan, S.; Yuan, Y.; Huang, Y.; Yang, Y.; Caffeine improves the performance and thermal stability of perovskite solar cells. *Joule* **2019**, 3, 1464-1477, doi:10.1016/joule.2019.04.005.
29. Liu, L.; Huang, S.; Lu, Y.; Liu, P.; Zhao, Y.; Shi, C.; Zhang, S.; Wu, J.; Zhong, H.; Sui, M.; Grain-Boundary "patches" by in situ conversion to enhance perovskite solar cells stability. *Adv. Mater*. **2018**, *30*, 1800544, doi:10.1002/adma.201800544
30. Lee, J. -W.; Dai, Z.; Han, T. -H.; Choi, C.; Chang, S. -Y.; Lee, S. -J.; De Marco, N.; Zhao, H.; Sun, P.; Huang, Y.; 2D perovskite stabilized phase-pure formamidinium perovskite solar cells. *Nat. Commun.* **2018**, *9*, 3021, doi:10.1038/s41467-018-05454-4.
31. Lee, J. W.; Bae, S. H.; Hsieh, Y. T.; De Marco, N.; Wang, M.; Sun, P.; Yang, Y.; A bifunctional Lewis base additive for microscopic homogeneity in perovskite solar cells. *Chem* **2017**, *3*, 290–302, doi:10.1016/j.chempr.2017.05.020.
32. Taguchi, M.; Suzuki, A.; Oku, T.; Fukunishi, S.; Minami, S.; Okita, M. Effects of decaphenylcyclopentasilane addition on photovoltaic properties of perovskite solar cells. *Coatings* **2018**, *8*, 461, doi:10.3390/coatings8120461.
33. Oku, T.; Kandori, S.; Taguchi, M.; Suzuki, A.; Okita, M.; Minami, S.; Fukunishi, S.; Tachikawa, T. Polysilane-inserted methylammonium lead iodide perovskite solar cells doped with formamidinium and potassium. *Energies* **2020**, *13*, 4776, doi:10.3390/en13184776.
34. Taguchi, M.; Suzuki, A.; Oku, T.; Ueoka, N.; Minami, S.; Okita, M. Effects of annealing temperature on decaphenylcyclopentasilane-inserted $CH_3NH_3PbI_3$ perovskite solar cells. *Chem. Phys. Lett.* **2019**, *737*, 136822, doi:10.1016/j.cplett.2019.136822.
35. Oku, T.; Taguchi, M.; Suzuki, A.; Kitagawa, K.; Asakawa, Y.; Yoshida, S.; Okita, M.; Minami, S.; Fukunishi, S.; and Tachikawa, T.; Effects of polysilane addition to chlorobenzene and high temperature annealing on $CH_3NH_3PbI_3$ perovskite photovoltaic devices. *Coatings* **2021**, *11*, 665, doi:10.3390/coatings11060665.
36. Oku, T.; Nakagawa, J.; Iwase, M.; Kawashima, A.; Yoshida, K.; Suzuki, A.; Akiyama, T.; Tokumitsu, K.; Yamada, M.; Nakamura, M. Microstructures and photovoltaic properties of polysilane-based solar cells. *Jpn. J. Appl. Phys.* **2013**, *52*, 04CR07, doi:10.7567/JJAP.52.04CR07.
37. Oku, T.; Nomura, J.; Suzuki, A.; Tanaka, H.; Fukunishi, S.; Minami, S.; Tsukada, S. Fabrication and characterization of $CH_3NH_3PbI_3$ perovskite solar cells added with polysilanes. *Int. J. Photoenergy* **2018**, 8654963, doi:10.1155/2018/8654963.
38. Suzuki A.; Taguchi M.; Oku T.; Okita M.; Minami S.; Fukunishi S.; Tachikawa T., Additive effects of methyl ammonium bromide or formamidinium bromide in methylammonium lead iodide perovskite solar cells using decaphenylcyclopentasilane, *J. Mater. Sci.: Mater. Electron.* **2021**, *32*, 26449–26464, doi:10.1007/s10854-021-07023-w.

39. Oku, T.; Zushi, M.; Imanishi, Y.; Suzuki, A.; Suzuki, K. Microstructures and photovoltaic properties of perovskite-type $CH_3NH_3PbI_3$ compounds. *Appl. Phys. Express* **2014**, *7*, 121601, doi:10.7567/APEX.7.121601.
40. Kishimoto, T.; Oku, T.; Suzuki, A.; Ueoka, N. Additive effects of guanidinium iodide on $CH_3NH_3PbI_3$ perovskite solar cells. *Phys. Status Solidi A* **2021**, *218*, 2100396. doi:10.1002/pssa.202100396.
41. Kandori, S.; Oku, T.; Nishi, K.; Kishimoto, T.; Ueoka, N.; Suzuki, A. Fabrication and characterization of potassium- and formamidinium-added perovskite solar cells. *J. Ceram. Soc. Jpn.* **2020**, *128*, 805, doi:10.2109/jcersj2.20090.
42. Nishi, K.; Oku, T.; Kishimoto, T.; Ueoka, N.; Suzuki, A. Photovoltaic characteristics of $CH_3NH_3PbI_3$ perovskite solar cells added with ethylammonium bromide and formamidinium iodide. *Coatings* **2020**, *10*, 410−1−10, doi:10.3390/coatings10040410.
43. Machiba, H.; Oku, T.; Kishimoto, T.; Ueoka, N.; Suzuki, A. Fabrication and evaluation of K-doped $MA_{0.8}FA_{0.1}K_{0.1}PbI_3$(Cl) perovskite solar cells. *Chem. Phys. Lett.* **2019**, *730*, 117–123, doi:10.1016/j.cplett.2019.05.050.